Implementing an on-line bond quality inspection system for cold roll bonded Al/Al-Sn/Al/steel strips using guided wave EMATs

Philipp J Tallafuss, Andrzej Rosochowski
Design, Manufacture and Engineering Management, University of Strathclyde
Glasgow, G1 1XJ, United Kingdom
+44 1563 55-8357
philipp.tallafuss@strath.ac.uk

Sylvia Campbell
MAHLE Engine Systems UK Ltd.
Kilmarnock, Ayrshire, KA1 3NA, United Kingdom

Xavier Minguez
Innerspec Technologies Europe S.L.
28802 Alcala de Henares, Madrid, Spain

Abstract

A prototype on-line bond inspection system for Al/Al-Sn/Al/steel strips is introduced to detect bond defects that occur in the cold roll bonding (CRB) process of strips. The transmitting and receiving ElectroMagnetic Acoustic Transducer (EMAT) probes inspect 100% material volume whilst the strip is processed continuously. The inspection signals are processed in real-time and are stored for post-processing. Serial production strips with good bond as well as with defects along the bond line were inspected for rigorous testing of the prototype machine. The inspection results were statistically analysed to determine an alarm threshold for serial inspection. The most important results are that the guided waves are sensitive enough for practical non-destructive testing (NDT) to detect all bond defects with only 0.5% false alarm rate, which nowadays can only be detected with a destructive peel-off test. The detection of all kinds of bond defects would lead to unreasonable levels of scrap due to false alarms. The application of this prototype EMAT inspection system to an industrial strip processing line shows that on-line detection of significant defects in CRBed Al/Al-Sn/Al/steel strips in a harsh serial production environment is possible. Design improvements are proposed to address the issues that occurred during inspection trials to design a more robust mechanical machine for the industrialisation of an EMAT inspection system.

1. Introduction

There is a need to develop an automated, on-line inspection technique to examine the bond of Al/Al-Sn/Al/steel strips produced by CRB. On-line implies that the inspection system is installed on a continuous production line as the Al/Al-Sn/Al/steel strip passes a fixed inspection point. Strips are used to manufacture engine sliding bearings in the automotive industry due to the ideal combination of properties of Al-Sn alloy and steel [1]. Figure 1(a) shows a micrograph of the four-layered Al/Al-Sn/Al/steel structure. The

cladding layers of the Al-Sn internal core are made of Al-1050 strip. The Al-Sn alloy has a nominal 6-20% tin content. The three-layered Al/Al-Sn/Al system is referred to as clad Al, which is CRBed onto steel free from aligned linear porosity or continous oxides. The backing is made of a low carbon steel. Figure 1(b) shows a micrograph of a delamination between the Al-1050 and steel interface that was detected during final inspection. Figure 1(c) shows a delamination defect that was detected while boring the inner diameter (ID) of a bearing, when the shear forces exceeded the adhesion between the layers. In CRB, the solid state weld is achieved by a substantial and simultaneous plastic deformation of the metals at room temperature [1]. The disadvantage is a large number of secondary operations and high requirements for bonding surface preparation [2], which are critical to bond quality. Current industry practice for inspection is destructive testing using a chisel test, peel test, shear test, Erichsen cup test or hot hammer test [1]. Although each technique has specific advantages and disadvantages, their major restriction is that only a minor proportion of the finished material is inspected. Automated on-line inspection could help to correct the problem during production to minimise scrap, avoiding value adding to defective material, reduction of business risk and financial losses if defects remain undetected and engine bearings fail in the field.

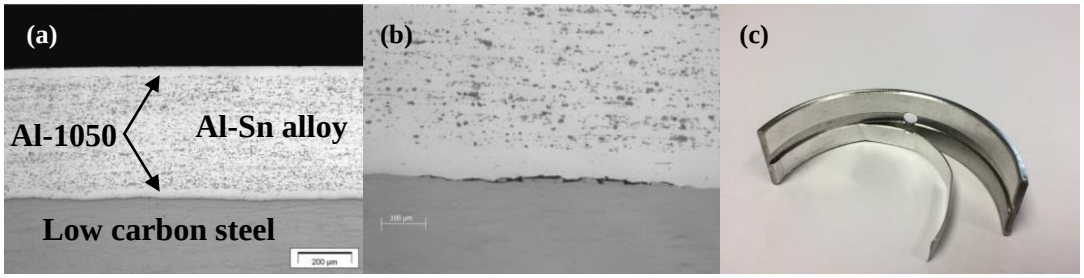

Figure 1. (a) Micrograph of the four-layered Al/Al-Sn/Al/steel structure with good bond, (b) delamination between Al-1050 and steel, (c) half shell bearing delamination

The result of a feasibility study using active thermography, shearography, ultrasound and guided wave EMAT NDT techniques to inspect the bond of Al/Al-Sn/Al/steel structures was that guided waves using EMATs is the most promising technique for on-line bond NDT [3]. A limitation of this research was that experiments were conducted under laboratory conditions instead of on-line in the harsh manufacturing environment. Subsequent research [4] has focused on guided waves and the detectability of delaminations, embedded steel debris and brittle intermetallic Al-Fe diffusion bond layers. It was found that the Sound-to-Noise (SNR) ratio is not significantly affected by post-rolling annealing, which suggests that on-line inspection can be done during production or post-rolling annealing in a final inspection line. This work builds on previous research outcomes [3], [4] and addresses the question of whether on-line inspection under the harsh manufacturing conditions is possible. A guided wave EMAT prototype inspection machine was designed and built in collaboration with an industrial partner. The system was deployed in a strip processing line for rigorous on-line inspection of full-length Al/Al-Sn/Al/steel strips. Typical guided wave EMAT inspection applications in industry are the inspection of pipes to detect corrosion or cracks [5], evaluation of the condition of rails [6], weld defect detection [7], adhesive bond inspection in composites [8] and metal plates [9], [10] and [11]. Furthermore it has

been reported that the technique has already been successfully applied in the inspection of three-layered cladding of brass/copper/brass material for coin stock [11]. However, no work has been reported to date on EMAT technology being used to inspect Al/Al-Sn/Al/steel strip on-line, when it is moving. The results of this study provide information about inspection repeatability, wave mode sensitivity to qualitatively indicate the occurrence of bond defects, and further system improvements for a serial inspection system.

2. General inspection system design

2.1 System requirements

The system must meet the following performance characteristics for on-line inspection:

I) Industrial CRB capability (rolling speed: 5 to 15 m/min and harsh manufacturing environment such as vibrations and shape deviations during processing)
II) Ability to detect serial production bond defects
III) Maximum strip width: ~ 300 mm
IV) Minimum strip width: ~ 170 mm
V) Maximum strip thickness: ~ 4 mm
VI) Minimum strip thickness: ~ 1.5 mm
VII) Display and export of historic records

2.2 General design of system

Figure 2 shows the strip processing line used for the experiments. The pneumatic brake disc uncoiler provides back tension. The roller table avoids strip oscillation. A rolling mill guides the strip to the EMAT probes. The transmitting and receiving probes, remote signal conditioning boxes, pneumatic and electrical components are mounted onto a probe assembly frame, which is positioned directly below the strip. Pneumatics provide passive compliance between probes and moving strip. Wear plates that are in sliding contact with the steel cover the probes. Remote signal conditioning boxes process and connect the probes to the Data acquisition (DAQ) hardware and computer with programmable temate® software. A coiler provides front tension and coils the strip after inspection.

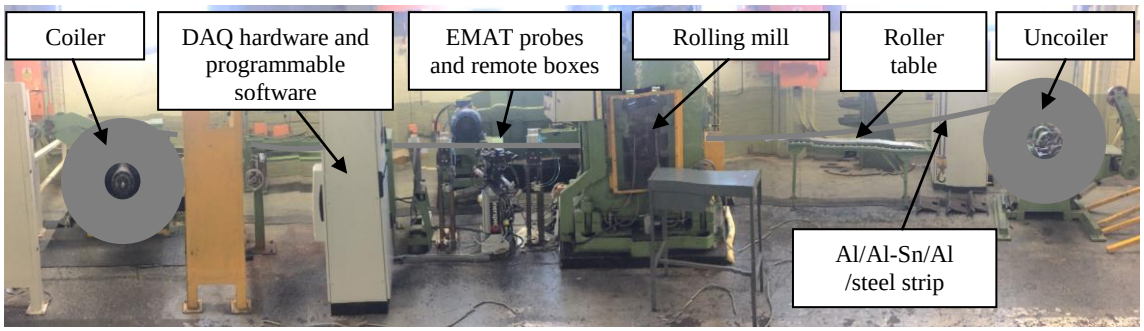

Figure 2. EMAT prototype inspection line for Al/Al-Sn/Al/steel strips

Signals are processed and displayed in real time. Figure 3 shows the interface of the temate® software. Figure 3a) illustrates the A-scan oscilloscope that is used to verify the selected wave mode, adjust gains and set signal inspection gates. Figure 3b) represents the maximum amplitude within the TOF filtering gates along the strip in real time during inspection. Once inspection is completed, the results can be retrieved in the recall panel (Figure 3c). In these modes, measurement locations, signal amplitude, indication of the pass/fail status depending on alarm threshold, and current strip identification data can be analysed. The ultrasound signals are measured in voltage and are displayed as relative amplitude as a percentage of the reference amplitude for a defect-free sample. The gain remains unchanged for all measurements.

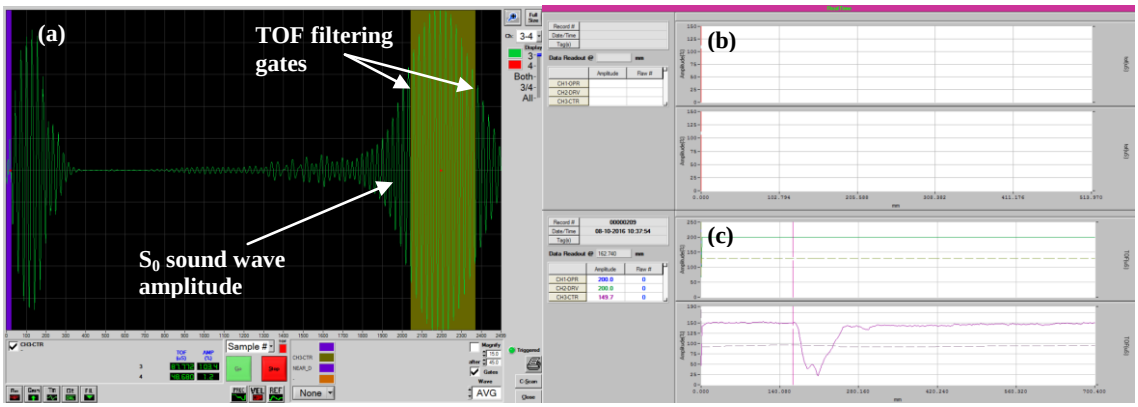

Figure 3. Temate® software a) A-scan oscilloscope, b) on-line A-scan maximum amplitude trace, c) A-scan maximum amplitude recall panel

3. Experimental procedure

3.1 Guided wave propagation and analysis

The inspection experiments were set up in the pitch and catch configuration as shown schematically in Figure 4(a). The transducers were positioned at the steel side on opposite sides of the strip.

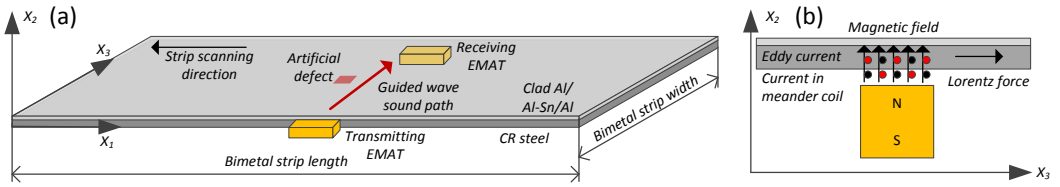

Figure 4. EMAT transducers to generate and receive guided waves in plates: (a) sound path, (b) interaction with material

Figure 4(b) is a schematic of the EMAT transducer and its interaction with the bimetallic sample. The transmitting and receiving transducers each have a magnet in the housing and a meander coil over the magnetic pole. Above the magnetic pole, the magnetic field (B) is mainly in the X_2 direction. Eddy currents (J) are induced by the

meander coil in the X_1 direction. The Lorentz force (f), which acts on particles in the sample due to the magnetic field (B) and eddy currents (J), is given by Equation 1:

$$f = J\ x\ B \text{ ----------(1)}$$

Since the current sent along the meander coil is periodically distributed, the corresponding eddy currents in the steel surface of the bimetallic sample generate periodically distributed loading. When the guided wave propagates above the receiving EMAT, the horizontally polarized stress field that it produces interacts with the magnetic field, thus generating currents in the meander coil, which is placed between the bimetallic sheet and the magnet. Each layer of the clad Al and steel sheets is assumed isotropic in the simulation of guided wave propagation dispersion curves, which are based on the general theory of elastodynamics [12], represented by a displacement equation of motion (Equation 2):

$$(\lambda + \mu)u_{j,ji} + \mu u_{i,jj} + \rho f_i = \rho \ddot{u}_i \text{ ----------(2)}$$

λ and μ are Lamé's first and second coefficients and depend on the Young's modulus and Poisson's ratio of the material in each layer. The displacement field is u, ρ is the density and f is the distributed body force. The coordinate directions are indicated with the indices i and j, in which 1 refers to the direction of wave propagation, 2 refers to the direction of the wave front, and 3 refers to the thickness direction. Table 1 summarises the material properties considered for the guided wave propagation analysis. The Rayleigh-Lamb phase and group velocity dispersion curves for this study were calculated using the semi-analytical finite element method (SAFE) and identified various wave modes that appeared to be good candidates for inspection. Figure 5(a) plots the phase velocity and Figure 5(b) plots the group velocity dispersion curves for the four-layer system. Excitation lines for the wavelengths used are drawn on the phase velocity dispersion curve. The wave mode at the intersection between the excitation line and the phase velocity dispersion curve will be efficiently excited when the corresponding frequency is used. Figure 5 shows the selected wave modes for this study. Since the prototype system discussed in this article will be industrialised as a commercial product, the wavelengths and frequencies of the employed wave modes are not revealed. The wavelength was controlled by the period of the meander coil.

Each wave mode was tested using A-scans with defect-free and artificially implanted defective samples to determine the wave mode sensitivity to defects and select the employed wave modes accordingly. Figure 6 shows example A-scans for 211 mm wide, 0.52 mm Al/Al-Sn/Al and 1.08 mm thick steel bimetallic plates, (a) without defects and (b) with 10x10 mm area embedded steel debris. An inspection gate between 42 and 46 μs was set for the through-transmission signal to monitor the amplitude changes. In Figure 6(a) the gain was adjusted to obtain a good bond reference amplitude. In Figure 6(b) the signal amplitude dropped significantly to 30% of the reference amplitude due to the defect.

Table 1. Material properties for Al/Al-Sn/Al/steel structure and employed guided wave modes

Material type	Characteristics	Clad Al/Al-Sn/Al			Backing material	Employed wave mode
I	Material	Al-1050	AlSn20CuMn	Al-1050	CR steel	1
	Height (mm)	0.04 +/- 0.01	0.64	0.04 +/- 0.01	2.06	
	Width (mm)	206	206	206	206	
	Density (g/cm^3)	2.71	3.12	2.71	7.8	
	Young's modulus (GPa)	70	70	70	203	
	Poison's ratio	0.33	0.33	0.33	0.293	
II	Material	Al-1050	AlSn6Si2CuNiMnV	AlMnSi	CR steel	2
	Height (mm)	0.04 +/- 0.01	0.52	0.04 +/- 0.01	1.58	
	Width (mm)	279	279	279	279	
	Density (g/cm^3)	2.71	2.82	2.73	7.8	
	Young's modulus (GPa)	70	70	70	203	
	Poison's ratio	0.33	0.33	0.33	0.293	
III	Material	Al-1050	AlSn10Si4Cu	Al-1050	CR steel	1
	Height (mm)	0.04 +/- 0.01	0.91	0.04 +/- 0.01	2.19	
	Width (mm)	206	206	206	206	
	Density (g/cm^3)	2.71	2.90	2.71	7.8	
	Young's modulus (GPa)	70	70	70	203	
	Poison's ratio	0.33	0.33	0.33	0.293	
IV	Material	Al-1050	AlSn6Si2CuNiMnV	Al-1050	CR steel	2
	Height (mm)	0.04 +/- 0.01	0.65	0.04 +/- 0.01	1.45	
	Width (mm)	227	227	227	227	
	Density (g/cm^3)	2.71	2.82	2.71	7.8	
	Young's modulus (GPa)	70	70	70	203	
	Poison's ratio	0.33	0.33	0.33	0.293	

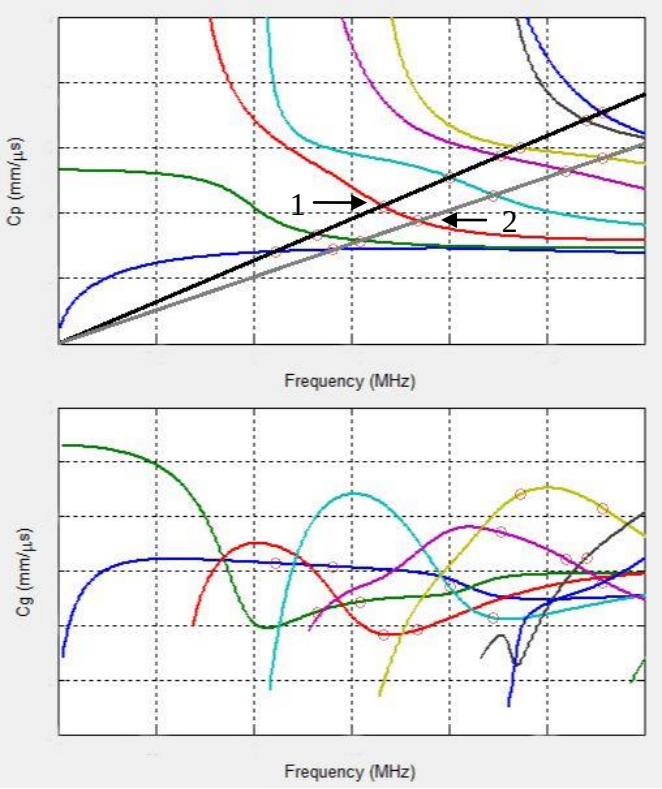

Figure 5. Dispersion curves of the four layer structure: (a) phase velocity with employed wave mode, (b) group velocity

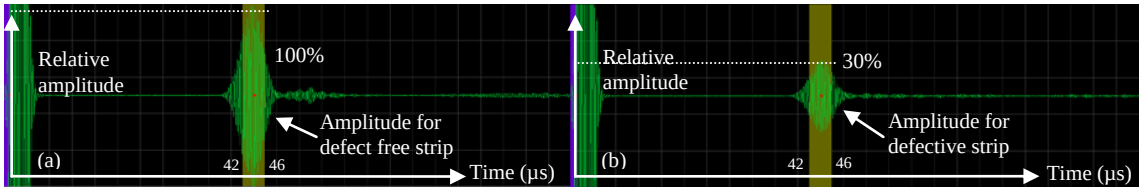

Figure 6. A-scan for (a) defect free and (b) defective Al/Al-Sn/Al/steel plate

The empirical relationship between bond defects and guided waves in all experiments was when guided waves encounter a bond defect, the defect causes destructive interference which converts incident wave energy into radiation energy in all directions, which results in attenuation. The remaining wave energy that propagates to the receiving EMAT transducer decreases, which is measured and shown as a lower signal amplitude in the A-scan. During inspection, the maximum amplitude within the TOF filtering gates is used to indicate defective material with the attenuation method.

3.2 Sample production

All Al/Al-Sn/Al/steel strip samples in this study were produced at the CRB production line at MAHLE Kilmarnock, Scotland. The process is schematically illustrated in Figure 7. Figure 7a) shows the Al/Al-Sn/Al cladding process. The cast Al-Sn alloy is straightened to allow mechanical surface preparation before cladding. The Al-Sn to Al-1050 interface, which faces the steel at CRB, is linished. The sacrificial side is wire brushed. Surface preparation is critical for the quality of the Al-1050 to Al-Sn bond. The Al-1050/Al-Sn/Al-1050 strips, stacked on top of each other, simultaneously enter a rolling mill, in which they experience a significant thickness reduction which creates cold welds. In a sequence of rolling passes, the clad Al is reduced to the final thickness (Figure 7b) before being CRBed to the steel (Figure 7c). The steel strip is degreased and the bond interface is mechanically activated by linishing. The clad Al bond surface is wire brushed immediately before CRB. Various studies [13], [14] have reported that this surface preparation of alloy and steel creates the strongest cold welds during CRB, because it removes contaminants and surface oxides that could interfere with the creation of nascent metal. The steel surface linishing creates a larger amount of surface asperities, which promotes localised shear deformation to break the unavoidable surface oxide films [15]. MAHLE plant trials substantiate that there is a negative effect on the bond integrity if the steel surface is not linished before CRB. Once prepared for CRB, the clad Al and steel strips enter the CRB mill simultaneously at a constant output speed of about 13 m/min and cold welds between the two materials are produced as a result of the significant thickness reduction. Typical unwanted particles at the bond interface in serial production at this stage are rolled-in steel debris, brush bristles and alloy slivers. The bonded strip is post-rolling annealed to recrystallize the grain structure of the work-hardened clad Al and enhance the bond between the Al-1050 and steel layers by diffusion.

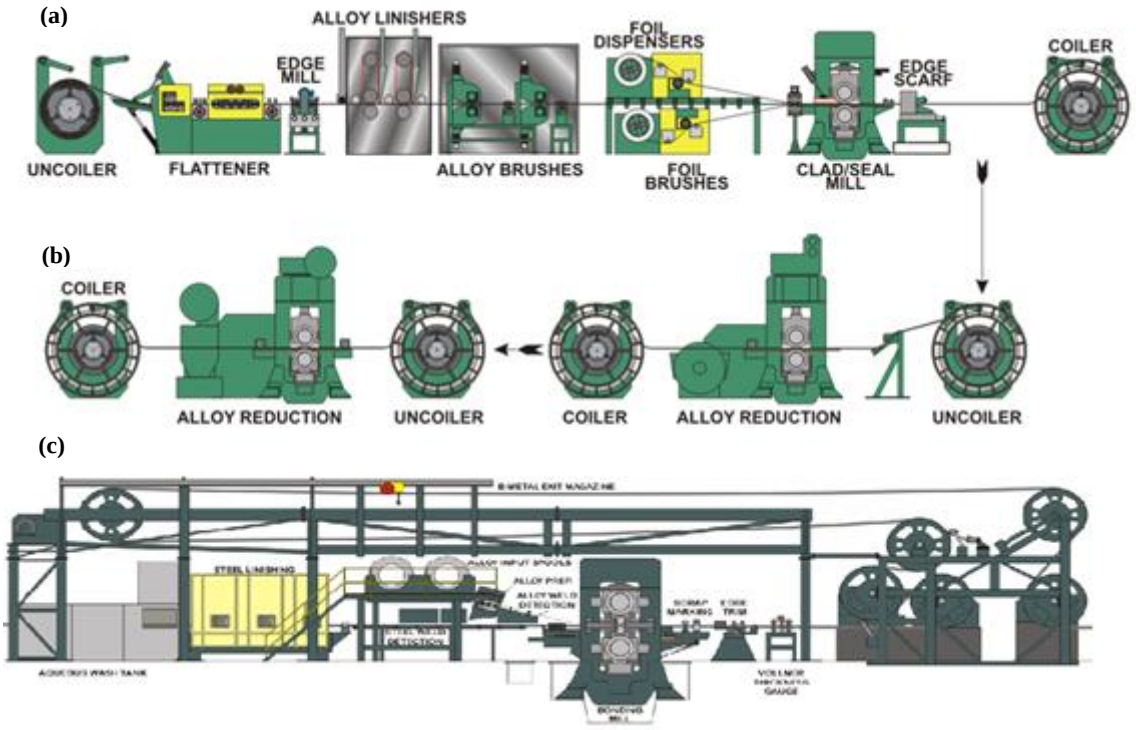

Figure 7. Al/Al-Sn/Al production process: (a) Al/Al-Sn/Al cladding, (b) clad Al rolling, (c) CRB of clad Al to steel

Table 2 summarises the test samples in this study. SP-R1 and SP-R2 are serial production reference samples that were produced without defects. SP-D is a 80 m long serial production strip with Al-1050 sacrificial side foil blisters. Artificial defects (AD) were implanted in the AD strip. The AD-T sample is the first 28 m in the AD strip, which were bonded when the mill roll temperature was only 42°C compared to the required temperature of above 100°C. Once at temperature, the next 28 m were bonded under normal process parameters to obtain a good bond reference sample (GBR). Samples AD-1x1D and AD-5x5D contain artificially implanted 1x1 mm and 5x5 mm area delaminations (D) by spreading a thin alumina powder layer on the steel surface before CRB. Steel debris (SD) was artificially implanted in samples AD-1x1SD and AD-5x5SD. The clad Al and steel strips were misaligned when entering the CRB mill to produce a sample with run-off alloy (ROA) on one edge of the strip and bare steel on the other side. The steel surface linishing before CRB in sample AD-ASS was intermittent due to a removed 50 x 150 mm area location in the rotating linishing belt, which produced locally altered steel sanding (ASS) parameters. Rolled-in alloy slivers (RAS) and rolled-in brush bristles (RBB) were artificially implanted between the clad Al and steel in the AD-RAS and AD-RBB samples. In order to obtain altered clad Al brushing (ACB), 50 mm of the wire brush width were deactivated across the circumference by bulging the bristles so as not to mechanically activate the clad Al surface. For reduced rolling reduction (RRR), the CRB thickness reduction was set to only 30% instead of the standard thickness reduction of >40%. For each sample in the AD strip, approximately 0.5 m length of the clad Al before and after each defect was ball-indented to mark scrap and locate the position of the artificial defect. The process stops with strip in the roll gap cause an imprint, which is also scrap. This imprint is present in the AD strip whenever the line was stopped to implant an artificial defect.

These roll mill stops (RMS) were also inspected. In between each artificial defect segment, approximately 10 m good bond strip was produced to keep the work rolls at temperature.

Table 2. Al/Al-Sn/Al/steel strip samples for on-line inspection

Strip	Sample #	Sample reference	Nominal alloy composition	Dimensions (clad Al/steel/width) (mm)	Strip length (m)	Approx. position from start (m)	Sample preparation
SP1	1	R1	AlSn20CuMn	0.64/2.06/206	320	-	Serial production reference 1
SP2	2	R2	AlSn6Si2CuNiMnV	0.52/1.58/279	390	-	Serial production reference 2
SP3	3	D	AlSn10Si4Cu	0.91/2.19/206	80	continuous	Serial production defect: Al-1050 blisters
AD	4	AD-T	AlSn6Si2CuNiMnV	0.65/1.45/227	160	0	Roll temperature 42°C
AD	5	AD-GBR	AlSn6Si2CuNiMnV	0.65/1.45/227	160	28	Good bond reference
AD	6	AD-1x1D	AlSn6Si2CuNiMnV	0.65/1.45/227	160	55	1x1 mm area delamination
AD	7	AD-5x5D	AlSn6Si2CuNiMnV	0.65/1.45/227	160	68	5x5 mm area delamination
AD	8	AD-1x1SD	AlSn6Si2CuNiMnV	0.65/1.45/227	160	81	1x1 mm area steel debris
AD	9	AD-5x5SD	AlSn6Si2CuNiMnV	0.65/1.45/227	160	90	5x5 mm area steel debris
AD	10	AD-ROA	AlSn6Si2CuNiMnV	0.65/1.45/227	160	100	Run off alloy
AD	11	AD-ASS	AlSn6Si2CuNiMnV	0.65/1.45/227	160	103	Altered steel sanding parameters
AD	12	AD-RBB	AlSn6Si2CuNiMnV	0.65/1.45/227	160	116	Rolled in brush bristles
AD	13	AD-RAS	AlSn6Si2CuNiMnV	0.65/1.45/227	160	117	Rolled in alloy slivers
AD	14	AD-ACB	AlSn6Si2CuNiMnV	0.65/1.45/227	160	140-142	Altered clad Al brushing parameters
AD	15	AD-RRR	AlSn6Si2CuNiMnV	0.65/1.45/227	160	144	Reduced rolling reduction to 30%
AD	16	AD-RMS	AlSn6Si2CuNiMnV	0.65/1.45/227	160	various	Rolling mill stop during bonding

Figure 8 shows the production of the artificially implanted defects immediately before CRB.

Figure 8. Defects in cold roll bonded Al/Al-Sn/Al/steel strips (a) 1x1 mm alumina, (b) 1x1 mm steel debris, (c) 5x5 mm alumina, (d) 5x5 mm steel debris, (e) run-off clad Al, (f) altered steel sanding, (g) rolled-in clad Al slivers, (h) rolled-in brush bristles, (i) altered clad Al brushing, (j) Al-1050 foil blisters on sacrificial side

3.3 Clad Al lining adhesion peel-back test

A clad Al adhesion peel-back test was used to obtain pass/fail measurement data for the test samples in this study to compare the results with the guided wave inspection. Figure 9 shows the test procedure, in which an incision through the Al/Al-Sn/Al lining is made with a sharp chisel, which is then prised upwards until it can be gripped with a pair of round-nosed pincers. Then the lining is peeled back in a rotational movement. The peel-back acceptability ratings were established empirically based on engine and field tests.

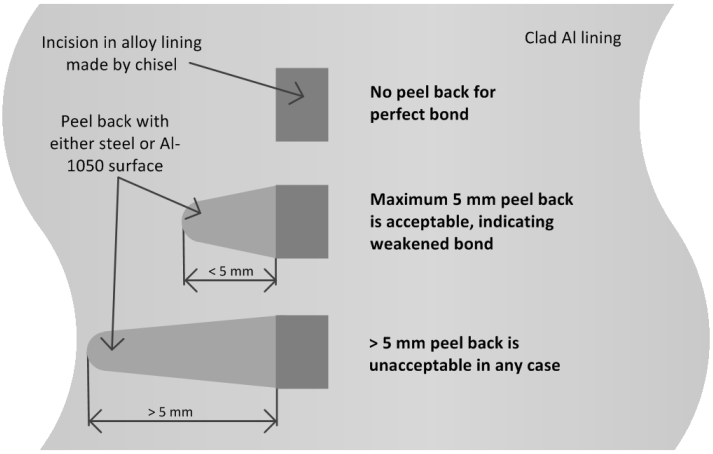

Figure 9. Clad Al lining adhesion peel back test procedure and pass/fail ratings

4. Results and discussion

4.1 *Data interpretation*

Figure 10 illustrates the measurement data interpretation approach in this study. The complete strip length of samples SP1-R1, SP2-R2 and SP3-D was scanned in one maximum amplitude trace without stopping the processing line. This is schematically illustrated in Figure 10(a) to (c). The same procedure was applied for samples AD-GBR, AD-T, AD-ASS, AD-ACB and AD-RRR, since the artificially implanted defects for these samples are several metres long.

For all other AD sample defects, which were artificially implanted at only a single position, one maximum amplitude trace was gathered per defect segment. Each segment consisted of approximately 10 m strip with good bond as reference, 0.5 m ball indentation scrap marking to indicate the beginning of the artificial defect, followed by the artificially implanted defect, and ending with 0.5 m ball indentation. Within each maximum amplitude trace, the artificially implanted defect scan was repeated 50 times to test the repeatability of the inspection system. The AD samples maximum amplitude trace in Figure 10d) shows 100 amplitude drops at the position of the artificially implanted defect, since recording continued whilst the strip was reversed. Only the measured amplitude in the forward direction was used for statistical analysis to control the strip front tension and eliminate any influence of lift-off between EMAT probe and strip.

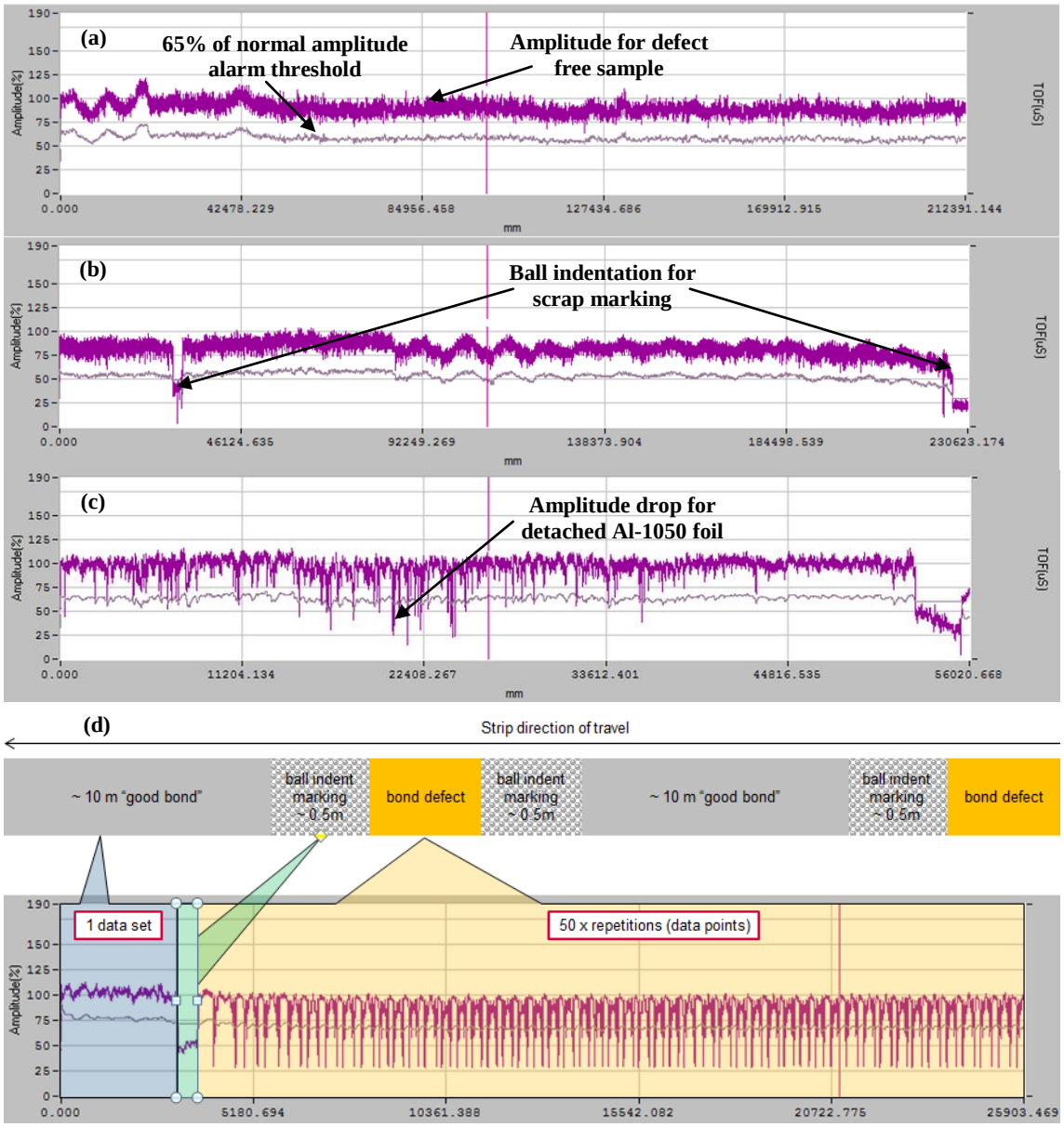

Figure 10. Results-based illustration of A-scan maximum amplitude trace: (a) SP1-R1 320 m, (b) SP2-R2 390 m, (c) SP3-D 80 m strips, (d) AD samples

A lower threshold of the normal amplitude level must be defined to detect bond defects. This threshold must avoid false alarms due to electrical noise and local material property variation, but still detect all potential defects. Therefore the mean amplitude for defects must be statistically significantly different from the good bond amplitude. If the amplitude intervals overlap, then no unambiguous differentiation between defective and good material is possible. In this case, setting the level of the threshold is a trade-off between not detecting real defects and reducing the false alarm rate. Sample SP3-D in Figure 10(c) shows that the signal amplitude drops below the alarm threshold at the locations where the Al-1050 foil detached from the AlSn alloy, which indicates the presence of defects. Since the exact locations and quantities of delamination spots in the serial production sample SP3-D were unknown, it was not considered in the statistical analysis.

4.2 Results

Figure 11 shows a boxplot of the SP and AD strip samples to compare the central tendency and variability of the measured amplitude for various defects. The interquartile range (IQR) from the first quartile (Q1) to the third quartile (Q3) shows that the middle 50% measurement points of all defects have a narrow spread. The IQR of the reference samples R1, R2 and GBR overlap. This was expected, since the reference samples were used to calibrate the system. All other measured amplitudes are normalised as the same gain was used to inspect the reference and defective samples. The range of the reference samples from the smallest to the largest amplitude value including outliers is from about 55% to 120% normalised amplitude. It can be seen that the combined interval of samples R1 and R2 completely contains the amplitude intervals of defective samples ASS, T, ACB and 1x1SD. These samples can therefore only be detected by accepting a significant false alarm rate. The sample RRR amplitude interval partly overlaps with the combined R1 and R2 interval, hence detection with a reduced false alarm rate is possible. Samples 5x5D, RMS, 1x1D, 5x5D, RBB, ROA and RAS amplitude intervals do not overlap with the combined R1 and R2 interval, therefore detection without false alarms is possible. The boxplot shows that the variances of the various samples are different.

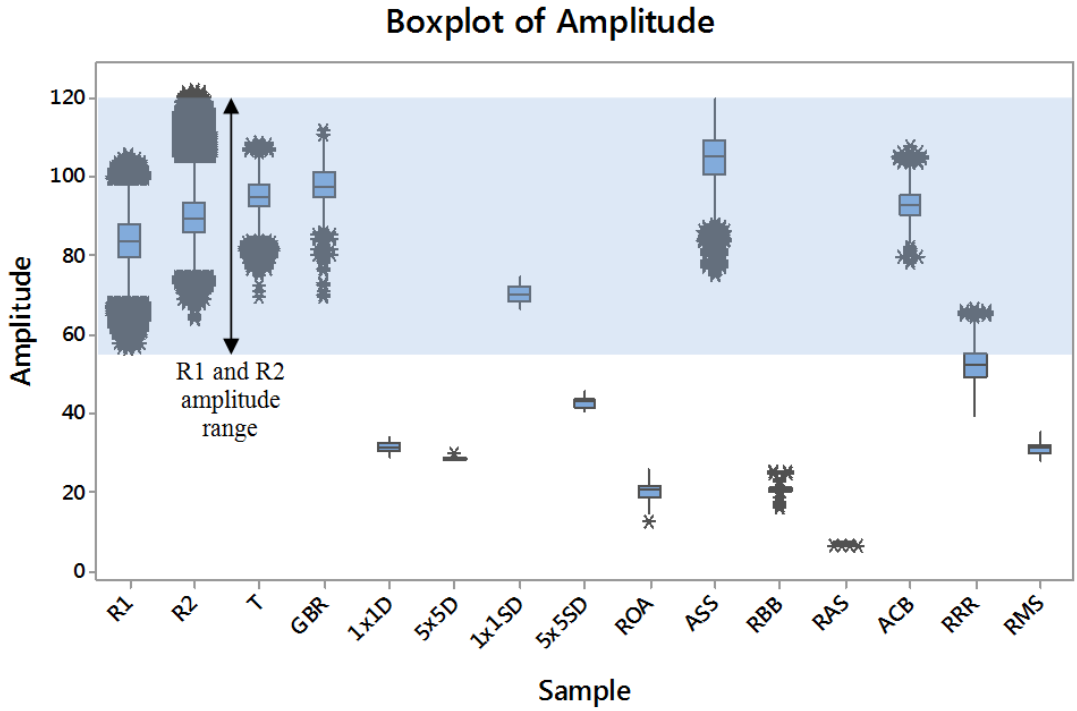

Figure 11. Boxplot of SP-R1, SP-R2 and AD strip samples showing central tendency and variability

Analysis of Variance (ANOVA) was used to analyse if the various bond defects could be differentiated by their mean amplitude. An alarm threshold of the normal amplitude was determined based on statistical analysis of the measurement data. Welch's ANOVA was identified as the applicable ANOVA test in this study, since it can be used for samples with normal distribution and unequal variances.

Normal probability plots were generated that are shown in Figure 12 to check the normal distribution of the measurement data. The x-axis is transformed to plot a

cumulative normal density function in a straight line. The measurement data is plotted and transformed to standard normal values by using the mean and standard deviation of the measurement data. The data is normally distributed when the samples fall along the normal line. It is recognisable that samples T and ASS are right skewed. This can be explained by the way the samples were made. The roll temperature was cold at the beginning of CRB when sample T was produced and then gradually increased to the operating temperature, hence the bond quality along sample T is different. For sample ASS, as shown in Figure 8(f), the unlinished area at the edge of the strip is not continuous along the length of the strip, but intermittent since only parts of the rotating linishing belt were removed to alter the linishing parameters. Therefore the local un-linished areas, with different signal amplitude, were measured repeatedly, which skewed the sample data distribution. ANOVA is insensitive to the normality assumption for large sample sizes, which applies for samples ASS and T. It can be seen that all samples fulfil either the normally distributed or large sample size criterion, and therefore Welch's ANOVA can be used.

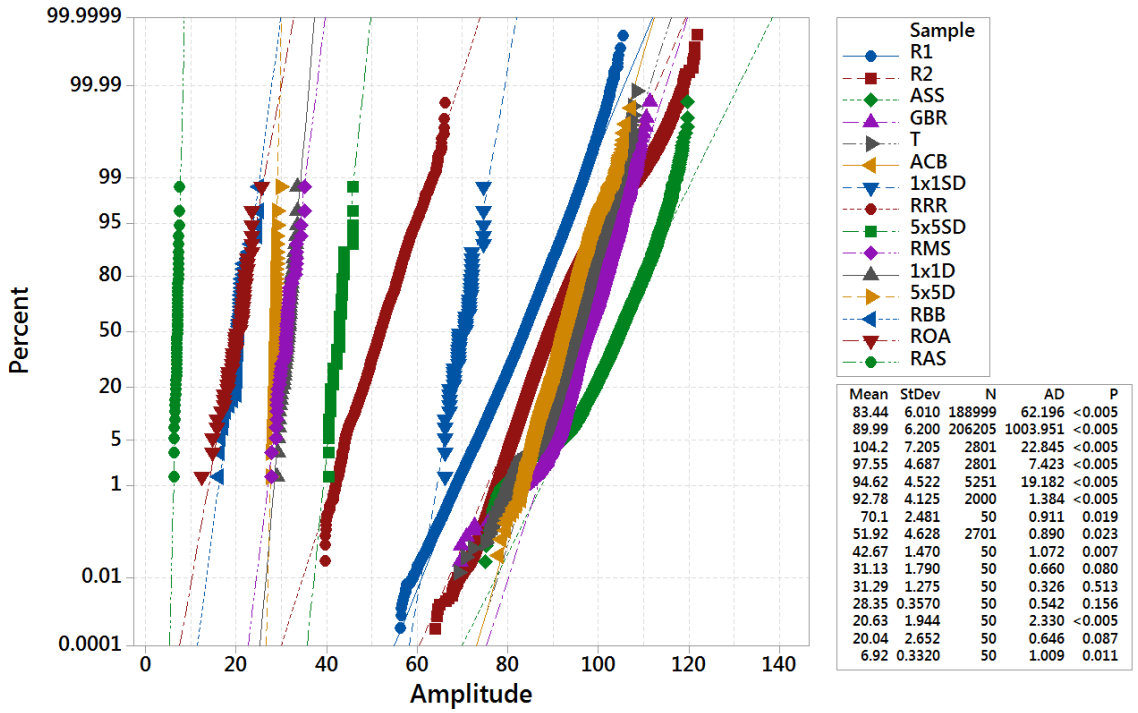

Mean	StDev	N	AD	P
83.44	6.010	188999	62.196	<0.005
89.99	6.200	206205	1003.951	<0.005
104.2	7.205	2801	22.845	<0.005
97.55	4.687	2801	7.423	<0.005
94.62	4.522	5251	19.182	<0.005
92.78	4.125	2000	1.384	<0.005
70.1	2.481	50	0.911	0.019
51.92	4.628	2701	0.890	0.023
42.67	1.470	50	1.072	0.007
31.13	1.790	50	0.660	0.080
31.29	1.275	50	0.326	0.513
28.35	0.3570	50	0.542	0.156
20.63	1.944	50	2.330	<0.005
20.04	2.652	50	0.646	0.087
6.92	0.3320	50	1.009	0.011

Figure 12. Amplitude normal test plots

Levene's test was used to test the homogeneity of variance of the samples. The null hypothesis (H_0) states that the variances are the same for all defects. The alternative hypothesis (H_a) is that at least one of the defective samples has a significantly different variance. The p-value is 0.000, hence H_0 must be rejected and the variances are significantly different. This is in line with the box plots in Figure 11, in which the different box lengths and whiskers for each sample indicate different variances. Welch's ANOVA test can be used for samples with different variances.

The null hypothesis for Welch's ANOVA is that all sample means are the same (μ = defect mean):

$$H_0 = \mu_{R1} = \mu_{R2} = \mu_D = \mu_T = \mu_{GBR} = \mu_{1x1D} = \mu_{5x5D} = \mu_{1x1SD} = \mu_{5x5SD} = \mu_{ROA} = \mu_{ASS} = \mu_{RBB} = \mu_{RAS} = \mu_{ACB} = \mu_{RRR} = \mu_{RMS} = \mu_k \quad (3)$$

The Welch's ANOVA results are Welch's F(14,461.175) = 315281.13, p = 0.000 and are summarised in Table 3. The p-value = 0.000 means that H_0 must be rejected and the alternative hypothesis (H_a) that there are at least two defect means that are statistically different from each other has to be accepted. Therefore the Games-Howell pairwise comparison post-hoc test [16] can be used to determine which specific samples are different from each other. This test can be used with unequal variances and unequal sample group sizes. The grouping results are summarised in Table 3. Differences between the means that share a letter are not statistically significant and therefore cannot be differentiated. This is the case for samples RMS and 1x1D that share the letter E as well as the samples ROA and RBB which are both in group I. All other samples do not share a letter, hence their means are statistically significantly different and can be differentiated from each other.

Table 3. Welch's ANOVA and Games-Howell Pairwise Comparison post hoc results (Minitab 17.1.0 statistical software)

Welch's ANOVA results

Source	DF Num	DF Den	F-Value	P-Value
Sample	14	461.175	315281.13	0.000

Games-Howell Pairwise Comparisons post hoc results

Sample	N	Mean	StDev	95% CI	Grouping
R1	188999	83.438	6.0102	(80.7404, 80.8163)	A
R2	206205	89.9866	6.2004	(89.9597, 90.0132)	B
T	5251	94.6202	4.5219	(94.3724, 94.8680)	C
GBR	2801	97.5498	4.6867	(97.2105, 97.8891)	D
1x1D	50	31.29	1.275	(30.928, 31.652)	E
5x5D	50	28.352	0.357	(28.2505, 28.4535)	F
1x1SD	50	70.1	2.481	(69.395, 70.805)	G
5x5SD	50	42.67	1.47	(42.252, 43.088)	H
ROA	50	20.042	2.652	(17.503, 22.581)	I
ASS	2801	104.238	7.205	(103.971, 104.505)	J
RBB	50	20.042	2.652	(19.288, 20.796	I
RAS	50	6.92	0.332	(6.8257, 7.0143)	K
ACB	2000	92.7775	4.1255	(92.5966, 92.9584)	L
RRR	2701	51.9228	4.6282	(51.7482, 52.0974)	M
RMS	50	31.132	1.79	(30.623, 31.641)	E

The result of the Welch's ANOVA and Games-Howell pairwise comparisons post-hoc test is that all samples, except for pairs 1x1D and RMS, as well as ROA and RBB, have statistically significantly different means and therefore can be differentiated. The disadvantage of this analysis is that it can be done only after inspection of the complete strip. In order to qualitatively indicate the occurrence of bond defects in real time, the attenuation method that was introduced above can be used. In this method defects are qualitatively indicated when the amplitude falls below a threshold of the normal amplitude and no unambiguous differentiation between defect types is possible. The criterion for the optimal threshold level is to minimise the false alarm rate due to electrical noise and local material property changes, and maximise the number of defect types that can be detected.

4.3 Determination of alarm threshold

The relationship between false alarm rate and threshold of the normal amplitude to detect defects was investigated to determine a reasonable threshold. A comparative study of a simple exponential moving average (EMA) (equation 4), a weighted moving average (WMA) (equation 5) and a simple moving average (SMA) (equation 6) was done. The EMA indirectly takes all previous measurement points into account and a smoothing factor α = 0.25 was used. For WMA, m = 10 weights (w_1 = 1/55, w_2 = 2/55, w_3 = 3/55, w_4 = 4/55, w_5 = 5/55, w_6 = 6/55, w_7 = 7/55, w_8 = 8/55, w_9 = 9/55, w_{10} = 10/55) were assigned to the ten most recent measured amplitude values. For SMA, m = 50 previous measured values were considered. The purpose of the moving average alarm threshold is to filter outliers and consequently reduce or avoid the false alarm rate. The same sample data from above was used for this study. The following equations were used:

$$\hat{y}_{t+1|t} = \alpha y_t + (1-\alpha)\hat{y}_{t|t-1} \text{----------(4)}$$

$$\hat{y}_i = (w_m y_{i-m} + \cdots + w_1 y_{i-1})/m \text{----------(5)}$$

$$\hat{y}_i = \frac{1}{m}\sum_{j=i-m}^{i-1} y_i = (y_{i-m} + \cdots + y_{i-1})/m \text{----------(6)}$$

Figure 13 plots the SP-R1 sample false alarm rate depending on the alarm threshold for the different averaging techniques. The false alarm rate is calculated as the number of occurrences in which the calculated amplitude value based on the averaging technique falls below the defined alarm threshold, divided by the total number of measured amplitude values per sample. This calculation is based on the assumption that the good bond reference sample SP-R1 is free of defects. The criterion for the selection of the averaging technique is to minimise the false alarm rate. The SMA technique offers the smallest false alarm rate. Considering that a false alarm rate of 0.50% is reasonably acceptable, then the alarm threshold should be defined as 65% of the normal amplitude level for the SMA technique. This point P(65.3%/0.50%) for the SMA technique is marked on the graph. For the same 65% alarm threshold, the WMA false alarm rate is 1.23%, EMA is 1.58% and for the unchanged data set it is 1.69%. Therefore the measurement data should be processed with the SMA technique during inspection to reduce the amount of rejected material due to false alarms.

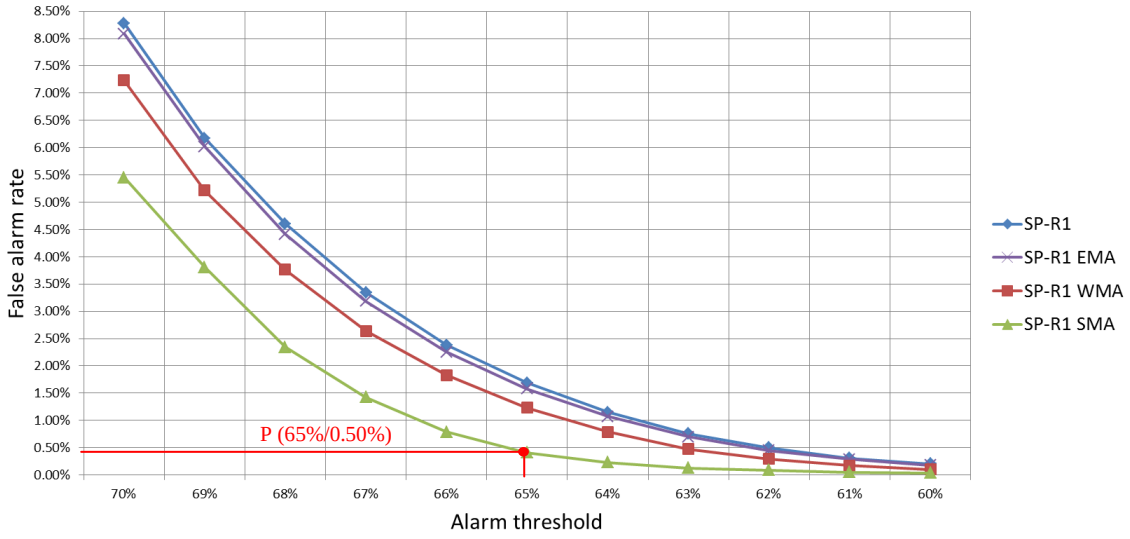

Figure 13. Relationship between false alarm rate and threshold for defect-free sample SP-R1

4.4 Detectability of main bond defects

The detectability of defects depends on the alarm threshold. Table 4 summarises the defects that are detectable in serial inspection with the attenuation method, if a 65% alarm threshold is used. Samples SP-D, AD-5x5D, AD-5x5SD, AD-ROA, AD-RBB, AD-RAS and AD-RMS can be detected on-line with guided waves as well as with the destructive peel off test. Samples AD-1x1D and AD-RRR can be detected on-line with guided waves, but are likely to remain undetected with the destructive peel off test because the peel-off is still below the fail rating. Defects AD-T, AD-GBR, AD-1x1SD, AD-ASS and AD-ACB cannot be detected with the 65% alarm threshold, but the same defects cannot be detected with the destructive peel-off test either. Based on a 65% alarm threshold, on-line inspection with guided waves offers the detection of more defect types than with the destructive peel-off test, and at the same time 100% material volume on-line inspection.

Table 4. Comparison between clad Al lining adhesion peel off and guided waves non-destructive test results, considering 65% of the normal amplitude alarm threshold and 0.50% false alarm rate

Sample #	Sample reference	Guided waves detectability	Peel off tets detectability	Peel off (mm)	Test correlation
1	SP-R1	x	x	1	✓
2	SP-R2	x	x	1	✓
3	SP-D	✓	✓	visual	✓
4	AD-T	x	x	1	✓
5	AD-GBR	x	x	1	✓
6	AD-1x1D	✓	x	2-3	x
7	AD-5x5D	✓	✓	>5	✓
8	AD-1x1SD	x	x	1	✓
9	AD-5x5SD	✓	✓	>5	✓
10	AD-ROA	✓	✓	visual	✓
11	AD-ASS	x	x	1	✓
12	AD-RBB	✓	✓	visual	✓
13	AD-RAS	✓	✓	visual	✓
14	AD-ACB	x	x	1-2	✓
15	AD-RRR	✓	x	1	x
16	AD-RMS	✓	✓	visual	✓

4.5 Improvements for serial system

Rigorous testing of the guided wave prototype inspection machine revealed that various machine modifications are necessary before the machine is capable of serial CRB inspection. A frequently occurring issue was lift-off between strip and EMAT probe. Huang et al. reported that lift-off between EMAT probes and samples are typically restricted to below 3 mm due to the requirement of a reasonable SNR. In this study, lift-off up to 20 mm occurred, in particular when the strip showed one-side waviness. In a serial system, the lift-off must be controlled to prevent false alarms. This could be done with a more flexible probe assembly design that is capable of maintaining a defined gap, or a strip guidance system such as a three-roll steering stand to correct the strip movement without deflection of the strip. A further limitation of the current prototype system is that the position of the defects across the width of the strip cannot be localised, which results in a low yield because the full width of the strip has to be scrap marked. It is common practice in engine bearing manufacturing that strips are slit into multiple strands in downstream processes. If the system resolution could be improved to locate the exact position of the defect, the yield could be improved by scrapping only the lane that contains the defect. A recent development in guided wave inspection of metallic plates is to attempt to accurately determine the location, size and shape of defects instead of only detecting the presence of defects. This is possible by using an array of transducers to transmit and receive guided waves from all directions [9], which would be an improvement compared to the current system that uses only one sound path across the width of the strip. Strip irregularities such as notches, steel and clad Al weld seams can damage the EMAT probes, if they remain undetected. A potential solution could be to integrate the bond inspection equipment into a machine visual inspection line that detects surface flaws. The machine visual inspection system could provide a signal to the bond inspection system to remove the sensor probes from the material when an irregularity arrives to prevent any damage. The current system uses different wave modes for strips with different dimensional characteristics. This requires EMAT meander coils with different coil periods. As a result of the different required inspection set-ups, time is required for the changeover from one part to another before inspection can begin. Further work is required to reduce the number of different wave modes for inspection of the complete product portfolio.

5. Conclusions

An on-line bond inspection system, with a high degree of automation, using guided waves generated with EMATs, has been applied and researched under harsh industrial conditions in an industrial strip processing line for CRBed Al/Al-Sn/Al/steel strips. The EMAT equipment has successfully demonstrated the on-line detectability of bond defects. The amplitude means of the defective samples were statistically significantly different from the control samples. It was found that based on a 0.5% false alarm rate, the alarm threshold should be set at 65% of the normal amplitude. Based on this threshold, more defects were detectable with the on-line inspection system than are nowadays detectable with the destructive clad Al peel-off test. In addition 100% of the material is inspected on-line instead of only samples at the beginning and the end of each strip. The limitation of the system is that no unambiguous differentiation between defects is possible with the real-time attenuation method. A more complex measurement

data analysis method that considers the time of flight could be considered for quantitative defect detection in future work. The implementation of a serial inspection system will result in a significant business risk reduction that engine bearings fail in the field.

Acknowledgements

The authors would like to thank MAHLE Engine Systems UK Ltd. for their support in providing the test samples and plant resources as well as Innerspec Technologies Inc. for providing the measurement equipment used in the present study.

References

[1] L. Da Silva, M. El-Sharif, C. Chisholm and S. Laidlaw, "A review of the cold roll bonding of AlSn alloy/steel bimetal strips," in *Conference Metal 2014 proceedings* , Brno, 2014.

[2] M. Stolbchenko, O. Grydin, F. Nuernberger, A. Samsonenko and M. Schaper, "Sandwich rolling of twin-roll cast aluminium-steel clad strips," in *11th International Conference on Technology of Plasticity, pp. 1541-1546*, Nagoya, 2014.

[3] P. J. Tallafuss, A. Rosochowski and S. Campbell, "A feasibility study on different NDT techniques used for testing bond quality in cold roll bonded Al-Sn alloy/steel bimetal strips," *Manufacturing Review,* vol. 4, no. 4, p. 18, 2017.

[4] P. J. Tallafuss, A. Rosochowski, S. Campbell and A. R. Camacho, "Detection of bond defects in cold roll bonded Al/Al-Sn/Al/steel sheets using Lamb type guided wave EMATs," in *1st World Conference on Condition Monitoring*, London, 2017.

[5] H. J. Salzburger, F. Niese and G. Dobmann, "EMAT pipe inspection with guided waves," *Welding in the World,* vol. 56, no. 5, pp. 35-43, 2012.

[6] P. A. Petcher, M. D. Potter and S. Dixon, "A new electromagnetic acoustic transducer (EMAT) design for operation on rail," *NDT & E International,* no. 65, pp. 1-7, 2014.

[7] P. A. Petcher and S. Dixon, "Weld defect detection using PPM EMAT generated shear horizontal ultrasound," *NDT & E International,* vol. 74, pp. 58-65, 2015.

[8] K. Arun, R. Dhayalan, K. Balasubramaniam, B. Maxfield, P. Peres and D. Barnoncel, "An EMAT-based shear horizontal (SH) wave technique for adhesive bond inspection," in *AIP Conference Proceedings*, 2012.

[9] S. Huang, Z. Wei, W. Zhao and S. Wang, "A new omni-directional EMAT for ultrasonic Lamb wave tomography imaging of metallic plate defects," *Sensors,* vol. 2, no. 14, pp. 3458-3476, 2014.

[10] S. Dixon, C. Edwards and S. B. Palmer, "Recent developments in the characterisation of aluminium sheets using electromagnetic acoustic transducers (EMATs)," *Insight,* vol. 44, no. 5, pp. 274-278, 2002.

[11] H. Gao, S. Ali and B. Lopez, "Efficient detection of delamination in multilayered structures using ultrasonic guided wave EMATs," *NDT&E International,* vol. 43, pp. 316-322, 2010.

[12] J. Achenbach, Wave propagation in elastic colids, Evanston: Elsevier, 2012.

[13] H. D. Manesh and H. S. Shahabi, “Effective parameters on bonding strength of roll bonded Al/St/Al multilayer strips,” *Journal of Alloys and Compounds,* vol. 476, no. 1-2, pp. 292-299, 2009.

[14] M. Sahin, “Effect of surface roughness on weldability in aluminium sheets joined by cold pressure welding,” *Industrial Lubrication and Tribology,* vol. 60, no. 5, pp. 249-254, 2008.

[15] R. F. Tylecote, D. Howd and J. E. Furmidge, “The influence of surface films on the pressure welding of metals,” *British Welding Journal,* vol. 1, pp. 21-38, 1958.

[16] P. A. Games and J. F. Howell, “Pairwise multiple comparison procedures with unequal n's and/or variances: a Monte Carlo study,” *Journal of Educational Statistics ,* vol. 1, no. 2, pp. 113-125, 1976.

[17] Z. Su, L. Ye and Y. Lu, “Guided Lamb waves for identification of damage in composite structures: A review,” *Journal of Sound and Vibration,* no. 295, pp. 753-780, 2006.

[18] P. D. Wilcox, R. P. Dalton and M. J. Lowe, “Mode and transducer selection for long range Lamb wave inspection,” *Key Engineering Materials,* no. 167-168, pp. 152-161, 1999.